American Mineralogist, Volume 90, pages 1192–1202, 2005

Low-temperature illitization of smectite in the late eocene and early oligocene of the Isle of Wight (Hampshire basin), U.K.

J.M. HUGGETT[1,2] AND J. CUADROS[1,*]

[1]Department of Mineralogy, The Natural History Museum, Cromwell Road, London SW7 5BD, U.K.
[2]Petroclays, 15 Gladstone Rd., Ashtead, Surrey KT21 2NS, U.K.

ABSTRACT

Variegated palaeosols, which formed from weathering of clays, silts, and brackish to freshwater limestones, are present in the late Eocene-early Oligocene Solent Group of the Hampshire Basin, southern U.K. The detrital clay mineral suite is dominated by illite and illite-smectite with minor kaolinite and chlorite. In pedogenically modified (palaeosol) and evaporitic lacustrine clay-rich sediments, the proportion of illite in the illite-smectite is greater than in the non-pedogenically modified sediments, and where alteration is most intense, kaolinite and chlorite are absent. The smectite to illite transition has been investigated in the <0.5 μm fraction by XRD analysis (powder and oriented mounts), thermogravimetry (TG), analytical SEM, and chemical analysis of Fe^{2+}. Modeling of XRD data reveals that the illite-smectite is a mixture of compositions (overall 60–95% illite), *R*0, with high rotational stacking disorder. Dehydroxylation occurs mainly at 500 °C, but also at higher temperatures, indicating heterogeneous octahedral cation composition. Analytical SEM and chemical analysis of Fe^{2+} indicate that the illite to smectite transition occurs through Fe reduction in octahedral sites leading to increased layer charge, coupled with K fixation. The driving mechanism for what appears to be irreversible Fe^{3+} reduction is wetting (reducing) and drying (oxidizing) cycles in gley soil, in which reoxidation of reduced Fe is never complete.

INTRODUCTION

With a growing interest in future climate change, it is becoming increasingly important to understand past climate. Authigenic clay minerals formed at or close to the Earth's surface are likely to be sensitive indicators of the geochemical environment of deposition and diagenesis. The spatial and temporal distribution of authigenic clay minerals in continental settings is an important record of palaeoenvironmental and palaeoclimatic conditions (e.g., Singer 1984; Singer and Stoffer 1980). Authigenic, illite-rich illite-smectite (I-S) has been reported from a Carboniferous palaeosol (Robinson and Wright 1987) and fixation of K by smectite also has been reported to occur in recent polders in France (Velde 2003). Illitic clays from hypersaline alkaline lakes have been more widely described, and known occurrences range in age from Jurassic to recent (Gabis 1963; Singer and Stoffer 1980; Deconinck et al. 1988; Hay et al. 1991).

The data presented here is part of an on-going multidisciplinary study of the solent group, in the Hampshire Basin, U.K. Huggett et al. (2001) demonstrated that the illite-rich clay assemblages of the solent group became illite-rich as a consequence of seasonal wetting and drying of smectite-rich clay in gley soils. At several horizons within the solent group, illite has also formed with gypsum and calcite in ephemeral hypersaline alkaline lakes. Here, we analyze in detail one lacustrine and five palaeosol clay samples, to obtain further evidence of the mechanism(s) of low-temperature illite formation.

GEOLOGICAL BACKGROUND

The solent group (Isle of Wight; Fig. 1) is a succession of brackish and freshwater clays, sands, and thin freshwater limestones of late eocene to early oligocene age, with a maximum thickness of 200 m, preserved only in the central part of the Hampshire Basin, in southern Hampshire, and the Isle of Wight. The solent group represents the youngest Palaeogene strata present onshore in the U.K. An extensive review of all previous work on the Tertiary deposits of the Isle of Wight has been published by Daley (1999).

The Headon Hill Formation (the oldest part of the solent group) is 90 m thick in Whitecliff Bay (Fig. 2). The succession is conspicuously cyclic; each cycle includes: (1) laminated, shelly silts and silty clays deposited in quasi-marine, brackish, and fluviatile environments, overlain by (2) units including numerous palaeosols developed in freshwater silts and silty clays. Four such cycles are present. The palaeosols are predominantly gleys, very wet or waterlogged soils in which anaerobic conditions would have prevailed. More recently, most of the Headon Hill formation gleys have undergone seasonal wetting and drying. In those parts of the profile that periodically dry out allowing air to penetrate, green FeO-bearing minerals, mainly "green rust," are redeposited as red Fe_2O_3, hematite. This is the cause of the characteristic color mottling and is a process separate from the illitization. Slickensiding, which is widespread in both the gley and pseudogley soils, is caused by movement of peds (a block or crumb of soil) during wetting and drying (Fitzpatrick 1980). Calcite nodules and gypsum crystals formed during periods when evaporation exceeded precipitation (Ollier and Pain 1996). The

* E-mail: j.cuadros@nhm.ac.uk

0003-004X/05/0007–1192$05.00/DOI: 10.2138/am.2005.1674

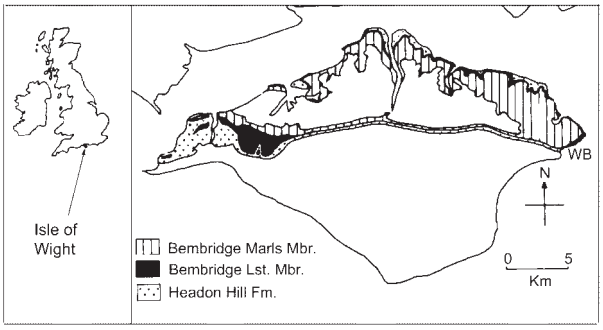

FIGURE 1. Map of the Isle of Wight with the outcrop of the lithologies described in the text; inset shows the location of the Isle of Wight in the U.K. WB = Whitecliff Bay.

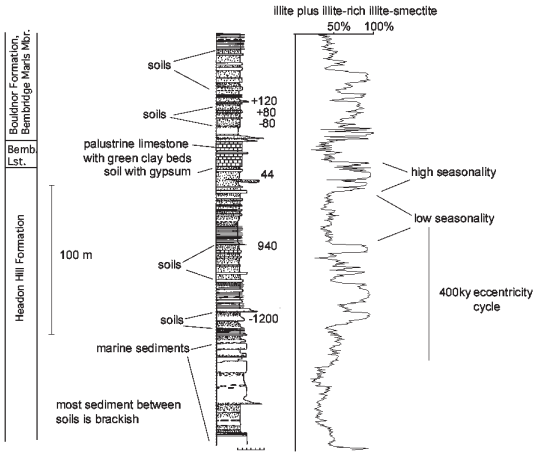

FIGURE 2. Lithological log of the interval of the Solent Group from which the samples were obtained. The graphic representation of illite plus illite-rich I-S abundance is for a much larger data set described in part by Huggett et al. (2001). These data are semi-quantitative, and are intended only to show the overall trend in illite layer abundance as they were derived by simple weighted means of peak areas.

C horizon is most often preserved, the A and B horizons less often, and the O horizon is absent in all cases (Huggett et al. 2001). Most of the soils show evidence of having been through more than one stage of development, i.e. gleying followed by seasonal drying out or vice versa. The Bembridge Limestone Formation (8 m), which succeeds the Headon Hill Formation, is made up of discrete beds of freshwater limestones, several of which are capped by palaeosols, alternating with beds of brackish and freshwater clay, deposited in palustrine (swampy) and lacustrine environments (Armenteros et al. 1997). The Bembridge Marls sees a return to clastic deposition with subsequent pedogenic modification.

MATERIALS AND METHODS

Six samples (+120, +80, –80, +44, +940, and –1200), selected to show a range of I-S abundance and expandability were selected from a 740 sample set.

Sediment composition

In mixed salinity and permanently water-logged gley environments (samples +80, +940, –1200), the clay assemblage comprises a wide range of I-S compositions, with minor kaolinite and rare chlorite. These sediments are brown, orange, red, or blue-green and they are commonly mottled. The blue-green sediments change to orange in a few weeks due to the presence of green rust. Clay assemblages dominated by illite-rich clays (samples +120, –80), are almost without exception gley or pseudogley palaeosols that are green (stable during the time since sampling which is up to 5 years) sometimes color mottled, slickensided, and calcareous (either nodular calcite or bioclasts). The detrital clay assemblage is derived from older smectite-rich Tertiary sediments in the Hampshire basin (Gale et al. 1999) that in turn were derived from older, Palaeozoic to Cretaceous sediments to the west (Gilkes 1968). This detrital clay contains I-S with a modal value of ~30% illite. This I-S was further illitized after deposition. As a consequence, there is a range of ages and I-S compositions represented in the samples analyzed here. This mixture of detrital I-S with pedogenically neo-formed I-S is the reason for the apparent Cretaceous and Jurassic K-Ar dates obtained by Huggett et al. (2001) for illite-rich samples. In the lacustrine Bembridge Marls, the clay fraction is almost pure illite with very minor kaolinite or I-S (sample +44). This clay is believed to be reworked from penecontemporaneous soils. Huggett et al. (2001) demonstrated that the illite in this sample is much more Fe-rich than the other samples, which could be due to Fe-enrichment in a hypersaline lacustrine environment. Apart from clays, the whole-rock mineralogy of all the clastic sediments is predominantly quartz, with occasional K-feldspar, ankerite, siderite, pyrite, and in the Bembridge Limestone Formation, bioclastic and authigenic calcite, plus calcite pseudomorphs after gypsum (Huggett et al. 2001). Halite and goethite were also identified by X-ray diffraction (XRD) but their presence is due to sea spray and oxidation of green rust, respectively.

The 001/002 intensity ratio of mica was measured on all samples (Huggett et al. 2001). This provides an indication of Fe content as Fe-rich micaceous clay has a weak 002 reflection. Values typically range from 1.48 to 7.8 and increase with the percentage of illite in the clay fraction (Fig. 8 in Huggett et al. 2001). The value measured for illite-rich marl from +44 is exceptionally high, at 12.1.

Experimental methods

The <0.5 μm fraction was separated by centrifugation to concentrate I-S. After drying, the samples were gently ground in an agate mortar. They were analyzed by thermogravimetry (TG) at the Istituto di Metodologie Per l'Analisi Ambientale (CNR, Potenza, Italy) using a Seiko Exstar 6000 apparatus. About 10 mg of clay were heated in Pt crucibles at 10 °C/min in an N_2 flow.

XRD analysis was performed on both oriented mounts and powder samples. The oriented mounts were prepared by dispersing ~100 mg of the clay in 2 ml of distilled water, placing the dispersion on a glass slide, and letting it dry. They were analyzed in the range 2–30 °2θ in a Philips PW1710 diffractometer at 45 kV and 40 mA, using a Cu anode, a graphite secondary monochromator, automatic divergence slit, and a 0.1 mm receiving slit. The samples were scanned at 0.015 °2θ step size and 3 s/step. The analyses were performed in both air-dry state (20–25 °C, 50–60% relative humidity) and following overnight glycolation at 60 °C in a glycol atmosphere. Powder analyses were performed in a Philips PW1050, at 42 kV and 42 mA, using a Cu anode, a graphite secondary monochromator, a 1° divergence slit and a 0.1 mm receiving slit. The samples were scanned in the range 19–44 °2θ to analyze illite stacking order, at 0.05 °2θ steps and 60–90 s/step. They were side-

loaded in an Si monocrystal holder (510 face) to enhance *hkl* over 00*l* peaks.

Chemical analyses were obtained by energy dispersive X-ray spectroscopy (EDS), using a JEOL 5900LV SEM equipped with an Oxford Instruments INCA EDS detector and with the use of mineral standards for calibration. The typical standard error is 1% of the concentration measured. Although less accurate than the ICP-AES data reported by Huggett et al. (2001), these data have the advantage of being for individual particles or clusters of particles rather than the bulk sample. A portion of each sample was dispersed in distilled water and a drop of the dispersion was placed on a carbon stub and allowed to dry. Analyses were performed on both particle aggregates of typical phyllosilicate flaky morphology and on isolated particles of similar shape. Data for further analysis were selected in two stages. First, those analyses with anomalous values for I-S were discarded; the remaining analyses were transformed into I-S structural formulae, assuming the anion composition $O_{10}(OH)_2$. Full tetrahedral occupancy was assumed, with Si + Al = 4. The remaining Al and all Fe, Mn, Ti, and Mg were assumed to be located in the octahedral sheet if the resulting occupancy was 2 or less. If the octahedral occupancy was > 2, the excess Mg was assumed to be in the interlayer, together with Ca, Na, and K. All Fe was included as Fe^{3+}, although it is known that there is Fe^{2+}. Then, analyses with Si < 3 and octahedral occupancy < 1.95 were removed, as indicating mineral contamination (see below).

The samples also were analyzed for Fe(II). For this, they were digested in HF/H_2SO_4 and the resulting solution titrated against potassium permanganate. Unfortunately, sample –80 was not available in sufficient amount to obtain a meaningful analysis. These results were not used to change the corresponding Fe analyses from EDS for two reasons. The first reason was that the EDS analyses correspond to individual particles and Fe^{2+} analyses to the entire sample. The second reason was that the Fe^{2+} values only amounted to 5–10% of total Fe.

TG analysis and XRD modeling

The first derivative of the TG diagram (DTG) was calculated to facilitate the location and interpretation of the thermal reactions. The DTG traces were analyzed in the region 250–800 °C to study the dehydroxylation reactions. For this, the diagrams were first deconvoluted and then decomposed in individual peaks using the Grams/32 package. The deconvolution process sharpens the individual peaks generating the overall DTG diagram and, hence, helps to locate them. In our study, many (but not all) of these individual peaks were observable before deconvolution. The peak positions were used to fix the peak maxima in the decomposition process (accomplished by curve fitting) in a first calculation. A straight baseline connecting the two minima at both sides of the dehydroxylation peaks was assumed and all peaks were modeled as Gaussian-shaped. In a second calculation, the peak positions were left free. All the calculations converged quickly to the final results and their total fitting standard errors were in the range 0.5–0.9%, calculated from the estimated standard errors of the peak positions, heights, and widths.

The oriented mount traces were modeled with NEWMOD (Reynolds and Reynolds 1996; Moore and Reynolds 1997), a program that allows calculation of 00*l* profiles for end-members and mixed-layer phyllosilicates with different interlayer complexes. First, the intensity of the experimental patterns was transformed from the automatic-slit profile to that of a fixed slit with the formula $I' = 2I_o/\sin\theta$ (where I' and I_o are the transformed and original intensities, respectively, and θ is the diffraction angle) to allow for a direct comparison between the experimental and calculated patterns. The NEWMOD calculations included the phyllosilicate phases present in the samples: I-S of different compositions, illite, and kaolinite. Several of these phases were mixed in the appropriate proportion. The other variables used to obtain the best match with the experimental patterns were composition of the I-S phases (% illite layers), their layer ordering (*R*) and interlayer hydration state (for the air-dry samples), Fe and K composition, and mean coherent scattering domain size. The orientation of the particles was set at σ* = 30° by best match with the experimental patterns, where σ* is the standard deviation from a 0° angle in a Gaussian distribution.

Two of the powder traces were modeled using WILDFIRE (Reynolds 1993), a program that calculates I-S and illite *hkl* profiles. The variables used were the dimensions of the mean coherent scattering domain in the **a**, **b**, and **c** directions, K and Fe composition, proportion of cis- and trans-vacant layers, and rotational disorder between layers. The layer rotational disorder is expressed using two variables: the proportion of layers with no rotation with respect to the previous layer (P_0) and that of rotated layers with 60° rotations or equivalent (180 and 300°, P_{60}). All coherently rotated layers that are not rotated 60° or equivalent angles are rotated 120 or 240°. Rotations different from the mentioned angles result in incoherent diffraction and the corresponding layers do not contribute to peak intensities. These rotations are considered random by WILDFIRE.

RESULTS

XRD analysis of oriented mounts

The experimental and simulated patterns of the air-dry and glycolated oriented mounts are shown in Figures 3 and 4, respectively. Samples +80, +940, –1200 and +120 contain mainly mixed-layer I-S, whereas samples –80 and +44 contain mainly illite. Other phases present are kaolinite (peaks at 12 and 25 °2θ), goethite (peak at 21 °2θ), calcite (peak at 29.5 °2θ), and quartz (sharp peaks at 21 and 26.7 °2θ in +940 only). The high intensity of the calcite peak in +940 is due to the fortuitous orientation of a crystal and does not correspond to its real abundance (see powder patterns below). The NEWMOD simulation of the patterns showed that the I-S phase was a complex mixture of several I-S phases with different smectite contents and coherent scattering domain thicknesses. We modeled these complex mixtures using a limited number of components (Table 1), but we believe that the samples consist of a mixture of numerous I-S phases, possibly including 3-layer components, within the range of smectite and illite compositions given in Table 1. Three-layer component mixed-layer clays have been described in several studies (e.g., Sakharov et al. 1999). As an example, to explain the results in Table 1, sample +80 in its air-dry state was modeled with 6 phases, of which 5 were I-S with differing expandability and one is kaolinite. The 6 phases were mixed in the indicated proportions but they are not mixed-layered with the other phases. In –80 and +44, there are illite grains of different coherent scattering domain size, which we modeled with two illite phases. The presence of several illite phases in these two samples is indicated by the sharpness of the upper part of the basal reflections and their broad bases. Our model is not intended as a completely accurate description of the complex samples but it is a good approximation of their clay mineral composition.

An important feature of these patterns is that I-S *R*0 predominates and is possibly the only ordering type. The difference between *R*0- and *R*1- or *R*3-type patterns of illite-rich I-S (95% illite in our simulations) is small and did not allow us to rule out $R > 0$ ordering in very illite-rich I-S in the samples. However, *R*0 and $R > 0$ patterns of I-S with 50–85% illite are substantially different and our calculations proved the presence of *R*0 and the absence of $R > 0$ ordering in I-S of this composition. Two areas in the patterns could not be simulated properly: 10–12 and ~26 °2θ. The intensity in the experimental patterns was higher in these two ranges than in the simulated patterns. We suspected that this is due to the presence of kaolinite-smectite (K-S). It could be possible that some K-S was associated with kaolinite. However, we discarded K-S from the calculations for two reasons. First, the amount of K-S needed to raise the pattern intensities in the 10–12 and 26 °2θ areas caused important misfits in other areas of the patterns, especially between 3 and 8 °2θ. Second, sample +44 does not have kaolinite although it does have a higher experimental intensity at 10–12 °2θ than the simulated pattern. Hence, K-S is evidently not the only possible reason for the discrepancy between the experimental and simulated patterns. The Fe contents, obtained by best match, indicate that, for samples +80, +940, –1200 and +120, the more illite-rich phases (within each sample) have lower octahedral Fe.

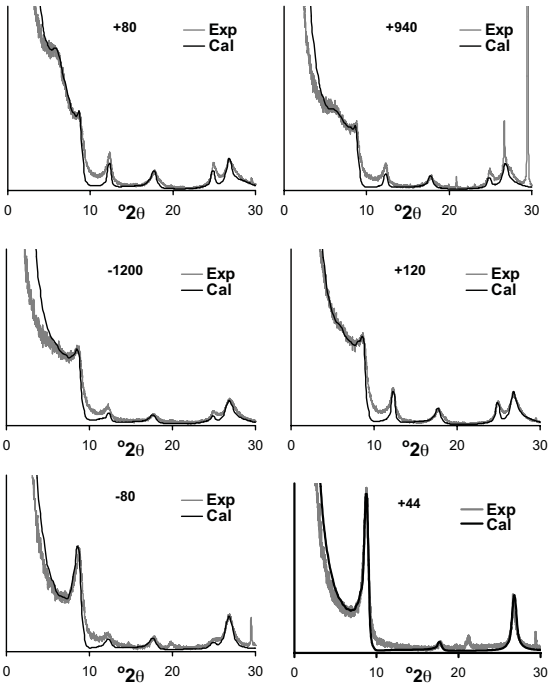

FIGURE 3. Experimental and calculated XRD patterns of the oriented, air-dry specimens.

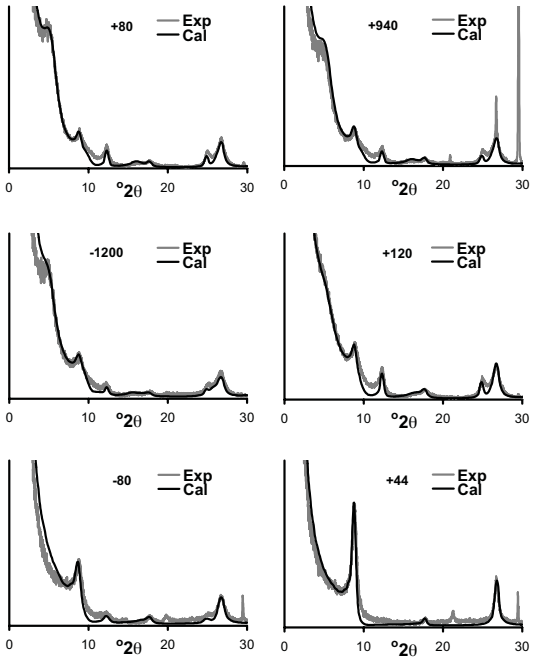

FIGURE 4. Experimental and calculated XRD patterns of the oriented, glycolated specimens.

Something similar is true for sample –80, where the illite phase with a larger coherent scattering domain has also a lower Fe content. Sample +44 stands alone, with the highest Fe content, the same for all I-S and illite phases.

TABLE 1. Parameters used in the NEWMOD calculations

Sample	Phase	%I	Air-dry d_s (Å)	Fe	N	N_{ave}	% Wt
+80	I-S_{40}	40	15	0.5	1–6	4	19
	Part coll I-S_{40}	40	12.4	0.5	1–6	4	13
	Part coll I-S_{75}	75	12.4	0.5	1–8	5	8
	Coll I-S_{75}	75	9.98	0.5	1–8	5	24
	Coll I-S_{95}	95	9.98	0	1–18	12	27
	Kaol				1–30	15	9
+940	I-S_{40}	40	14.5	0.5	1–6	4	12
	Part coll I-S_{40}	40	12.4	0.5	1–6	4	8
	Part coll I-S_{75}	75	12.4	0.5	1–8	5	20
	Coll I-S_{75}	75	9.98	0.5	1–8	5	21
	Coll I-S_{95}	95	9.98	0	1–18	12	32
	Kaol				1–30	15	7
–1200	I-S_{40}	40	15	0.5	1–6	4	6
	Part coll I-S_{40}	40	12.4	0.5	1–6	4	8
	Part coll I-S_{75}	75	12.4	0.5	1–8	5	17
	Coll I-S_{75}	75	9.98	0.5	1–8	5	32
	Coll I-S_{95}	95	9.98	0.3	1–14	9	30
	Kaol				1–30	15	7
+120	I-S_{40}	40	15	0.5	1–6	4	8
	Part coll I-S_{40}	40	12.4	0.5	1–6	4	8
	Part coll I-S_{75}	75	12.4	0.5	1–8	5	16
	Coll I-S_{75}	75	9.98	0.5	1–8	5	31
	Coll I-S_{95}	95	9.98	0	1–18	12	27
	Kaol				1–30	15	10
–80	Coll I-S	70	9.98	0.5	1–7	4	33
	$Illite_1$			0.5	1–5	3	16
	$Illite_2$			0.4	1–13	9	45
	Kaol				1–18	11	6
+44	Coll I-S	70	9.98	0.8	1–7	4	12
	$Illite_1$			0.8	1–5	2	15
	$Illite_2$			0.8	1–18	15	73
			Glycol (Kaol % as in air-dry)				
+80	I-S_{40}	40	16.9	0.5	1–6	4	45
	I-S_{75}	75	16.9	0.5	1–8	5	19
	I-S_{95}	95	16.9	0	1–18	12	27
+940	I-S_{40}	40	16.9	0.5	1–6	4	37
	I-S_{75}	75	16.9	0.5	1–8	5	23
	I-S_{95}	95	16.9	0	1–18	12	33
–1200	I-S_{40}	40	17.5	0.5	1–8	4	28
	I-S_{75}	75	16.9	0.5	1–8	5	39
	I-S_{95}	95	16.9	0.3	1–14	9	26
+120	I-S_{40}	40	16.9	0.5	1–6	4	11
	I-S_{75}	75	16.9	0.5	1–8	5	48
	I-S_{95}	95	16.9	0	1–18	12	31
–80	I-S	70	16.9	0.5	1–7	4	33
	$Illite_1$			0.5	1–5	3	16
	$Illite_2$			0.4	1–13	9	45
+44	I-S	70	16.9	0.8	1–7	4	12
	$Illite_1$			0.8	1–5	2	15
	$Illite_2$			0.8	1–18	15	73

Notes: Part coll = partially collapsed; %I = illite proportion in the corresponding I-S phase; d_s = d-value of smectite layers; Fe = in the corresponding phase per half formula unit; N, N_{ave} = range of number of layers and average number of layers in the coherent diffraction domain, respectively. Other parameters are: R (I-S) = 0; Illite d-value = 9.98; K in illite per half formula unit = 0.8; $\sigma^* = 30$.

All glycolated samples had homogeneous smectite *d*-values but the air-dry specimens showed variable smectite layer thickness. Hence, some of the smectite layers in the air-dry state were calculated as partially or completely collapsed. The abundance of these collapsed or semi-collapsed smectite layers increased with illite proportion in the sample. This is a frequent feature in smectite: all layers swell uniformly with glycol solvation but not with water solvation, where heterogeneous layer charge or interlayer cation composition become apparent. Ideally, the corresponding concentrations of the different phases modeled in the air-dry and glycolated state should match. There is a good match in the two most illite-rich samples (–80 and +44) and for I-S with 95% illite in all samples. However, there are large differences for the I-S phases with 40–75% illite layers. These differences

highlight that our calculations are only an approximation to a very complex mixture of phases with I-S crystals containing 40–100% illite layers. From this perspective, it is not meaningful to analyze the proportions of illite and smectite layers in each calculated phase and, rather than this, it is more appropriate to adopt a simplified view and analyze smectite and illite proportions in all I-S phases together.

Figure 5 shows the relative proportion of layer types in each sample. This plot was created by adding the contribution of each individual phase within a sample to each layer type (expanded, partially collapsed, and illite). For the glycolated specimens, only two layer types were observed: smectite and illite. In the air-dry specimens, however, the heterogeneous swelling behavior of smectite layers generates 3 smectite-layer groups: fully expandable (15 Å), partially collapsed (12.5 Å), and collapsed (10 Å). The collapsed smectite layers add to the true illite layers, from which they can be distinguished by glycolation but not in the air-dry state. Figure 5 suggests that some smectite layers (from ~5% of the total number of layers in +44 to ~25% in –1200) are in the process of illitization and have an increased layer charge and/or K content that diminish their swelling ability in the air-dry state (they appear as partially or totally collapsed), although they still swell fully when glycol-solvated.

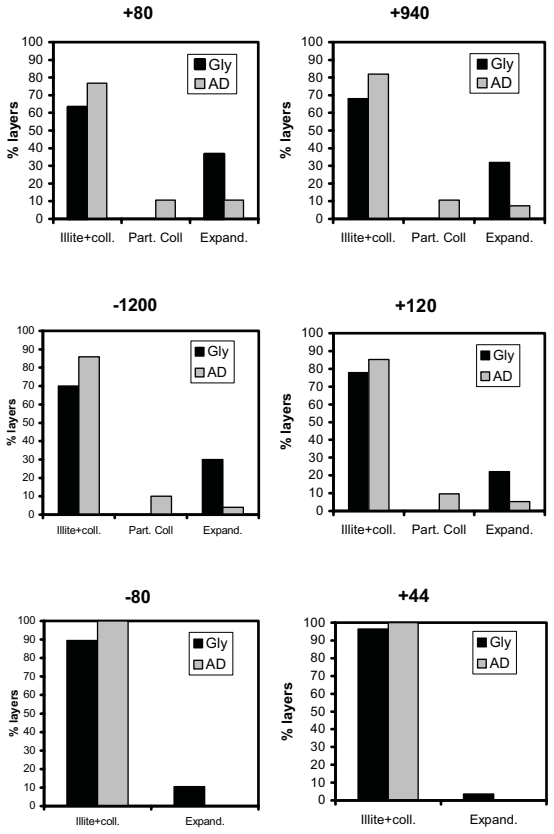

FIGURE 5. Relative proportion of layers (expandable, partially collapsed, and collapsed + illite) obtained from the NEWMOD calculations, for the air-dry and the glycolated patterns.

XRD analysis of powder mounts

The powder XRD analyses were intended to assess illite stacking order in I-S. The patterns (Fig. 6) show peaks from other phases that can be recognized by their sharper outline, except the kaolinite 002 peak (25 °2θ), which is also broad. The powder patterns indicated a low stacking order for all samples by the weak development of *hkl* ($h,k \neq 0$) reflections. As all patterns present similar development of these peaks, only two of them were modeled using WILDFIRE.

Table 2 shows the parameters that produced the best fit for samples +120 and +44. The percentage of illite layers corresponds to the weighted proportion of all I-S phases used in the previous NEWMOD calculations (Table 1). Iron content in I-S and K content in illite per half formula unit were selected by best match of the calculated and experimental patterns and they compare well with the selected values in the NEWMOD simulations (the only difference is in +120, with K = 0.8 and 0.7 in NEWMOD and WILDFIRE calculations, respectively). The degree of preferred orientation in the powder mount is indicated by the parameter *Or*, which varies between 1 in a completely random orientation and 0 in a perfect preferred orientation. The more smectite-rich samples show a less random orientation, noticed by the increased steepness of the areas at both sides of the I-S peak at ~27 °2θ. Due to the presence of the kaolinite, calcite, and halite peaks in these areas, it was not possible to assess the randomness of the particle orientation with great accuracy. The parameters *N* provide the average number (also maximum for N_c) of unit cells within the coherent scattering domain in the three crystallographic directions. N_a and N_b are lower than the usual values used for I-S of diagenetic origin (60 and 30, respectively; Reynolds 1993). The two N_c values for +44 are those derived from a lognormal distribution of coherent scattering domain thickness in I-S with 96% illite. However, for + 120, the N_c values in Table 1 are smaller than those provided by such lognormal distribution in I-S with 78% illite ($N_c$ave = 2.8, $N_c$max = 10). These values may indicate that the lateral dimensions (*a*, *b*) of the I-S crystallites are small in both samples, and that there are numerous crystallographic defects in the illite interlayers in sample +120 that decrease the thickness of the diffraction domains. The proportion of illite non-rotated layers relative to their neighbors, P_0 (range of possible values from 0.33 to 1), is the minimum for +44 and low for +120. This means that both have a high degree of rotational disorder. The layer rotations considered by P_0 correspond to 60° and multiple angles only. Any other rotation angle would cause a defect in the crystal and a boundary between scattering domains. The type of layer rotation is further specified by P_{60}, which indicates the proportion of layers rotated with angles 60, 180, and 300° (as opposed to 120 and 240°). In the two calculated patterns, 60° and 120° rotation types are equally abundant. Finally, both samples are mainly composed of cis-vacant layers (P_{cv}).

The above values cannot be considered totally accurate because the presence of other mineral phases is a hindrance for the simulations, but the similarity between the patterns and the low N_c and/or P_0 values prove that all the studied samples have a high degree of stacking disorder. The powder patterns show the presence of only one polytype ($1M_d$). This is important to note because the two illite phases modeled in the oriented mounts

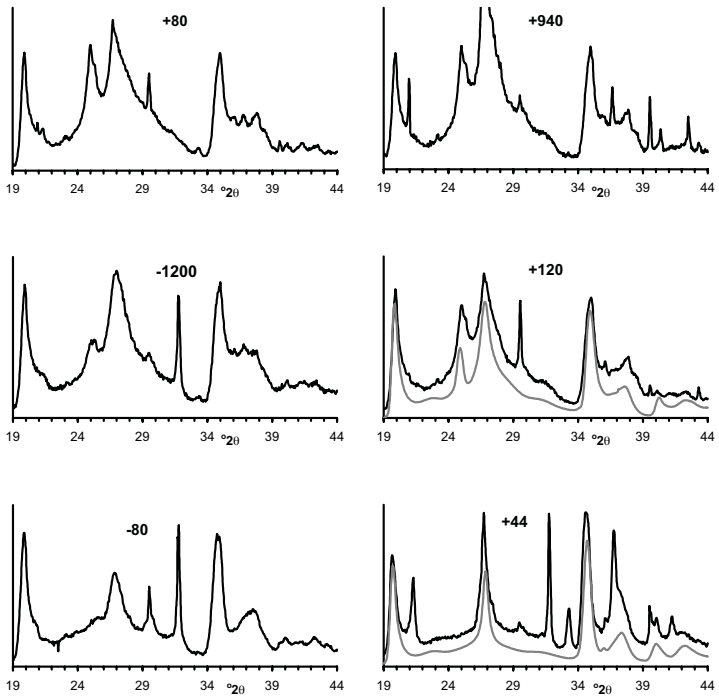

FIGURE 6. Powder XRD patterns of the I-S specimens. The corresponding calculated traces are shown in grey for +120 and +44. Peaks of mineral phases other than I-S are: kaolinite at 25 °2θ; quartz 21, 26.7 36.7, 39.6, 40.4, 42.5 °2θ (+80 and +940); calcite 29.6, 36.1, 39.5, 43.3 °2θ (the last 3 only observable in +120); halite 31.8 °2θ; goethite 21.3, 33.3, 36.8, 39.5, 40.1, 41.3 °2θ (in +44 and small amount in +80).

TABLE 2. Parameters used in the WILDFIRE calculations

Sample	%I	Fe	K	Or.	N_a	N_b	$N_c$ave	$N_c$max	P_{cv}	P_0	P_{60}
+120	78	0.33	0.7	0.9	40	20	2	5	0.9	0.5	0.5
+44	96	0.8	0.8	1	40	20	4.3	10	0.9	0.33	0.5

Notes: %I = % illite layers; Fe, K = composition per half formula unit; Or = degree of random orientation; N = number of unit cells in the coherent scattering domain for a, b, c directions; P_{cv} = proportion of cis-vacant layers; P_0 = proportion of non-rotated layers; P_{60} = proportion of layers rotated 60, 180, 300°.

of samples –80 and +44, one or more of high crystallinity and other/s of low crystallinity, could suggest that the high-crystallinity phase is detrital and originated by advanced diagenesis. Such illite phases commonly have $1M$-$2M_1$ polytypes. These powder patterns are more compatible with an illite source that produced crystals of a wide thickness range (coherent scattering domain along **c**). Obviously, the illite in the detrital I-S (that was then altered toward a more illitic composition) has a different origin, but this only accounts for an approximate maximum of 30% illite layers, whereas these samples have 90 and 96% illite layers. The illite in the detrital I-S was $1M_d$, as is usually the case with I-S of diagenetic origin with low illite content. The important point is that further illitization did not produce more-ordered illite polytypes, contrary to what usually happens in diagenetic illite.

Thermogravimetric analysis

The TG and DTG diagrams (Fig. 7) show two main weight-loss events, one from room temperature to below 200 °C and the other between 400 and 700 °C. The former is the loss of hydration water from the external surface and the smectite interlayers. The latter is the loss of hydroxyl water from I-S and kaolinite. Between the two, in the range 250–400 °C, there is another event observed in some of the samples, corresponding to goethite dehydroxylation. The I-S dehydroxylation event extends to a temperature higher than 700 °C in samples –80 and +44. The other three phases observed in the XRD patterns are calcite, halite, and quartz. Halite melts at ~800 °C and quartz undergoes the α→β transition at ~570 °C (Mackenzie 1957) with no weight loss and, hence, these reactions are not observed by TG. Calcite decomposes at 890–1010 °C (maximum of DTG peak; Mackenzie 1957). Some of the samples show a small weight loss above 800 °C (Fig. 7) that could correspond with calcite. In any case, the amount of calcite is so small that the effect in the TG and DTG diagrams is negligible.

We analyzed the dehydroxylation region in order to obtain structural information. Figure 8 shows the corresponding region and the results of the deconvolution and decomposition process used. Goethite dehydroxylation appears as one to three peaks of which one is sharp (311 and 305 °C in +80 and +44, respectively) and the other two rather broad. The kaolinite and I-S dehydroxylation region is complex, with several peaks of variable shape and position. The presence of two peaks at about 500 °C in all samples except +44 is not directly obvious but the deconvolution process always made both manifest. The sharper peak corresponds to kaolinite dehydroxylation and the broader one is part of the I-S dehydroxylation system. The relative proportions of kaolinite obtained from the DTG peak areas are in excellent agreement with those from XRD (Table 1). Dioctahedral I-S, smectite, and illite can dehydroxylate at different temperature in the range 500–650 °C (this range corresponding to the position of the peak maxima rather than to their full width)

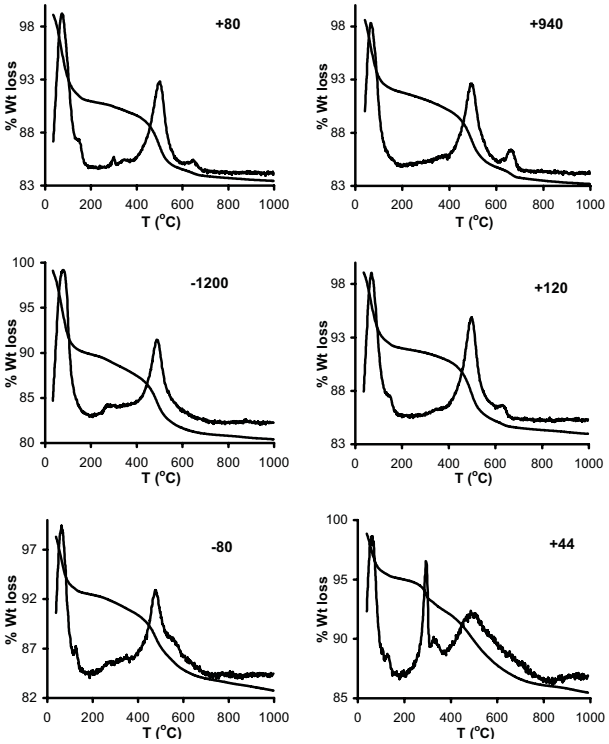

FIGURE 7. TG and DTG curves of the I-S specimens. The vertical scale corresponds to the weight loss in the TG curve.

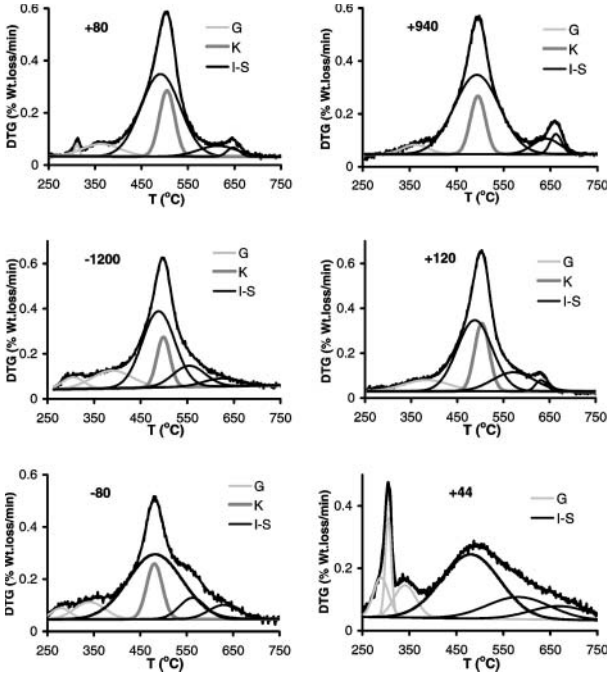

FIGURE 8. Decomposition of the DTG curve corresponding to dehydroxylation. The total reaction includes multiple dehydroxylation events for I-S and goethite (G) and one for kaolinite (K).

depending on structural factors such as the cis- or trans-vacant character of the octahedral sheet (Drits et al. 1995; Cuadros and Altaner 1998a) and to compositional factors such as Fe and Mg octahedral content (Heller-Kallai and Rozenson 1980; Muller et al. 2000).

Chemical analyses

Care was taken to perform the analyses in areas showing the typical clay morphology. Nevertheless, it was impossible to discriminate between kaolinite, which seemed to be fine-grained and evenly distributed within the samples, and I-S. Many analyses showed contamination from kaolinite and other minerals, the latter perhaps by grains below the clay particles. We used two criteria to select uncontaminated I-S analyses: after calculation of the corresponding structural formula, we selected those analyses with 3 < tetrahedral Si < 4, and 1.95 < octahedral occupancy < 2, per half formula unit. Very few analyses of samples +120 and –1200, and none of samples –80 and +44, passed these criteria.

The results are shown in Table 3 and, in Figure 9, as plots of Si, Fe and Mg vs. K per half formula unit. The only possible trend observed within samples (only +80 and +940 have enough data points for comparison within samples) is for the Fe-K data of sample +940, in which they might be positively correlated ($R^2 = 0.5$). There is no trend in the plots across all samples. This is remarkable for the Si-K plot because diagenetic I-S always displays a negative Si-K correlation. Thus, in these samples, the increase in layer charge that accompanies K fixation and illite formation is not produced by Al for Si substitution in the tetrahedral sheet. Neither is it due to Mg substitution for Al or Fe in the octahedral sheet.

The lack of Fe-K correlation within samples and the possible positive correlation for sample +940 do not support the XRD observation that the most illitic I-S phases within each sample have lower Fe content. However, each of the data points in Figure 9 corresponds to more than one I-S crystal and this may be blurring the actual Fe-K correlation. The K contents of 0.42–0.63 per half formula unit compare well with reported values for I-S with 60–80% illite of hydrothermal (Inoue and Utada 1983) and diagenetic origin (Cuadros and Altaner 1998b), although the Si contents in this work are below (0.4–0.15 atoms per half formula unit) those in Inoue and Utada (1983) and Cuadros and Altaner (1998b). This is probably due to the fact that our samples contain more Fe, because it is a trend in smectite, and probably also in I-S when it preserves part of the original smectite structure and composition, that increasing Fe content is coupled with decreasing tetrahedral Si (Cuadros 2002, and references therein.)

Fe^{2+} titration analysis produced the following FeO contents, in wt% (±0.02): +80 = 0.60, +940 = 0.37, –1200 = 0.39, +120 = 0.65, and +44 = 2.13. Sample –80 could not be analyzed for lack of material. The Fe^{2+} content increases with illite layer content except for sample +80, where illite layer proportion is low (Fig. 10, bottom).

DISCUSSION

The detrital clay-mineral suite of pedogenically unmodified Solent Group sediment is derived from older Eocene sediments (Gale et al. 1999) and is dominated by illite and smectite-rich

TABLE 3. Chemical EDS analyses transformed into structural formulae calculated per half formula unit

Sample	Si	Al^{IV}	Al^{VI}	Mg^{VI}	Fe III	Mn	Ti	Mg_{int}	Ca	Na	K	Σoct
+80	3.34	0.66	0.98	0.19	0.81	0.00	0.02	0.01	0.04	0.22	0.51	2.00
+80	3.31	0.69	0.97	0.17	0.82	0.00	0.03	0.03	0.03	0.20	0.49	2.00
+80	3.34	0.66	0.94	0.22	0.82	0.01	0.02	0.02	0.03	0.26	0.49	2.00
+80	3.34	0.66	0.92	0.14	0.90	0.00	0.03	0.04	0.06	0.06	0.52	2.00
+80	3.31	0.69	0.92	0.17	0.83	0.00	0.09	0.02	0.06	0.08	0.52	2.00
+80	3.31	0.69	0.92	0.15	0.90	0.01	0.02	0.04	0.05	0.08	0.54	2.00
+80	3.28	0.72	0.92	0.19	0.85	0.01	0.03	0.03	0.04	0.27	0.49	2.00
+80	3.29	0.71	0.95	0.17	0.86	0.02	0.02	0.03	0.04	0.26	0.47	2.00
+80	3.34	0.66	0.98	0.16	0.83	0.00	0.03	0.04	0.06	0.07	0.52	2.00
+80	3.34	0.66	0.98	0.16	0.83	0.00	0.03	0.06	0.05	0.05	0.51	2.00
+80	3.24	0.76	0.79	0.14	1.02	0.01	0.04	0.02	0.07	0.10	0.58	2.00
+80	3.28	0.72	0.94	0.16	0.87	0.01	0.03	0.05	0.04	0.16	0.52	2.00
+80	3.29	0.71	0.93	0.16	0.88	0.01	0.03	0.04	0.04	0.15	0.55	2.00
+80	3.35	0.65	0.92	0.16	0.90	0.00	0.02	0.02	0.01	0.19	0.53	2.00
+80	3.28	0.72	0.87	0.19	0.89	0.00	0.04	0.00	0.01	0.40	0.48	1.99
+80	3.32	0.68	0.93	0.19	0.85	0.00	0.02	0.01	0.02	0.31	0.47	2.00
+80	3.23	0.77	0.84	0.20	0.89	0.00	0.03	0.00	0.01	0.60	0.42	1.97
+120	3.39	0.61	1.03	0.17	0.71	0.01	0.03	0.00	0.02	0.27	0.58	1.96
+120	3.30	0.70	0.96	0.29	0.71	0.01	0.02	0.00	0.02	0.43	0.56	1.98
+940	3.30	0.70	0.85	0.19	0.90	0.00	0.02	0.00	0.02	0.41	0.54	1.96
+940	3.34	0.66	0.92	0.20	0.84	0.01	0.02	0.00	0.03	0.19	0.63	1.99
+940	3.33	0.67	0.88	0.18	0.86	0.00	0.04	0.00	0.04	0.27	0.59	1.96
+940	3.43	0.57	1.08	0.21	0.69	0.01	0.02	0.02	0.05	0.15	0.47	2.00
+940	3.36	0.64	0.98	0.22	0.76	0.00	0.01	0.00	0.01	0.39	0.53	1.97
+940	3.30	0.70	0.84	0.21	0.90	0.00	0.02	0.00	0.03	0.36	0.58	1.96
+940	3.36	0.64	0.95	0.21	0.82	0.00	0.02	0.00	0.04	0.22	0.55	2.00
+940	3.35	0.65	0.90	0.21	0.84	0.00	0.03	0.00	0.02	0.29	0.56	1.98
+940	3.32	0.68	0.92	0.20	0.81	0.00	0.03	0.00	0.02	0.33	0.57	1.97
+940	3.34	0.66	0.91	0.20	0.83	0.00	0.03	0.00	0.03	0.35	0.53	1.96
+940	3.35	0.65	0.96	0.23	0.76	0.00	0.02	0.00	0.02	0.41	0.51	1.97
–1200	3.13	0.87	0.62	0.22	1.10	0.02	0.01	0.00	0.02	0.53	0.62	1.97

illite-smectite with minor kaolinite and chlorite. Green and variegated green-red gley and pseudo-gley palaeosols formed on clay-rich brackish to lacustrine sediment. These pedogenically modified sediments are enriched in illitic clay relative to non-pedogenically modified sediment. This enrichment in illite cannot be ascribed to reworking of specific illite-rich beds as none are known from the sediment source area. This enrichment also precludes the interpretation that the smectite-rich beds are a result of smectitization of detrital illite-rich sediment. Illitization of smectite is a common feature of burial diagenesis, but burial of the Solent Group has not exceeded a few 100 m and this mechanism could not account for the selective illitization of clay in palaeosols. The mechanism inferred for smectite illitization in palaeosols (Robinson and Wright 1987; Huggett et al. 2001), calcrete (Watts 1980), and glass-rich silicic volcanic rocks (Gilg et al. 2003) is one of seasonal wetting and drying. This has been proposed based on experimental work (e.g., Mamy and Gaultier 1975; Eberl et al 1986; Šucha and Širáňová 1991) where smectite subjected to wetting and drying in the presence of K, NH_4, or Cs has been shown to undergo partial layer collapse. However, it is not clear whether these cations are necessarily fixed by this mechanism, which must therefore also involve increased layer charge, or whether the clay becomes a K, Cs, or NH_4 smectite. Abundant slikensides in the Solent Group palaeosols indicate that wetting and drying has occurred, whereas red-green mottling indicates partial oxidation or reduction, which may be a consequence of wetting and drying cycles (Huggett et al. 2001), presumably reflecting wetter winters and drier summers. The abundance of the pulmonate gastropod *Lymnaea* increases during these times of high seasonal contrast, probably because lymnaeids are air breathing and thus able to survive well in ephemeral water bodies (Paul 1989). Gypsum pseudomorphs also formed during periods of high seasonal contrast and support an overall picture of short-lived water bodies, drying out in summer and refilling in winter (Armenteros et al. 1997).

Illitization of smectite has also been reported from hypersaline environments with alkaline potassic pore fluid (Singer and Stoffers 1980; Deconinck et al. 1988) with cyclical wetting and drying (Deconinck et al. 1988). Potassium enrichment may occur through evaporation, marine ingression (Deconinck et al. 1988), or transformation of K/Na zeolite to analcime (Singer and Stoffers 1980). The first of these two mechanisms may be applicable to the illite enrichment that has occurred in lacustrine sediment toward the top of the Solent Group (sample +44). This is supported by the presence of calcite pseudomorphs after gypsum, the proximity of estuarine sediments and the presence of abundant *Lymnaea*.

The illitization process by wetting and drying operates initially by a simple mechanical layer collapse as K (also Cs and NH_4, but we will refer to K alone herewith as it is the cation found in the environment under study) becomes dominant in the interlayer (Eberl et al 1986; Cuadros 2002). In such a process, it is expected that the layers preserve much of the rotational disorder typical of smectite. Diagenetic illitization is usually accompanied by an increasing illite layer stacking order favored by increasing temperature, which allows faster evolution toward the most stable crystal structure. In supergene illitization, however, the much lower energy supply is likely to preclude noticeable layer rearrangement. This lack of rearrangment is consistent with the high degree of layer rotational disorder found in our samples (Fig. 6, Table 2) and their similar degree of disorder, even though they cover an overall range of 63–96% illite in I-S. For the reason mentioned, this illitization mechanism is also unlikely to produce structural changes within the layers. This lack of

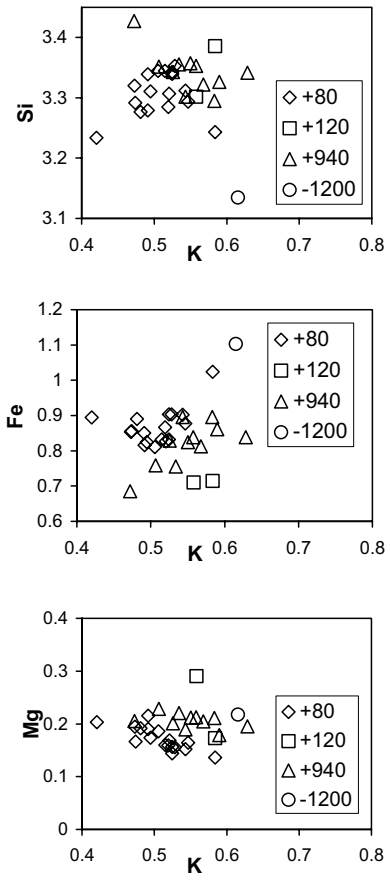

FIGURE 9. Chemical composition plots of I-S grains from the analytical SEM data, calculated per half formula unit. Data from samples –80 and +44 were contaminated with other mineral phases and are not shown. No trends are observed between Si-K, Fe-K, or Mg-K compositions.

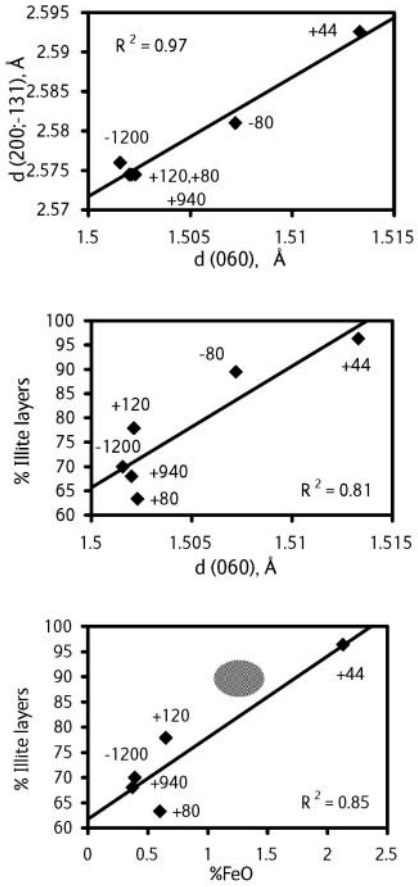

FIGURE 10. Plots of (1) top: the spacing of the 200, $\bar{1}31$ peak vs. that of the 060 peak, taken from the powder XRD patterns, (2) middle: overall percent illite layers in the samples vs. the spacing of the 060 peak, and (3) bottom: overall percent illite layers vs. FeO content. The grey area in the bottom plot indicates where sample –80 would most probably appear (see text).

structural changes is also consistent with the lack of cis-vacant to trans-vacant lattice transformation observed in our samples (Table 2), a transformation that is known to accompany illitization of Al-rich smectite in diagenesis (Drits et al 1996; Cuadros and Altaner 1998a).

Following the initial K exchange and layer collapse, there must be an increase in layer charge that generates the illite layers. The chemical data do not support either the usual process of Al for Si substitution in the tetrahedral sheet nor one of Mg for Al, Fe substitution in the octahedral sheet. Besides, the sample description indicates no atom rearrangement in the octahedral sheet and no changes in layer stacking. The lack of atom rearrangement at these two levels of the I-S structure supports the observed lack of chemical change. The effective mode of increasing layer charge without atom substitution is Fe reduction. Our I-S samples contain sufficient Fe (Table 3) to produce a noticeable layer charge increase by reduction of a fraction of their Fe. The Fe^{2+} content of the samples is in agreement with an illitization process driven by Fe reduction, as Fe^{2+} and illite content correlate well. This argument is discussed below.

Reducing conditions occur in water-saturated soils, and repeated wetting and drying is acknowledged to produce K fixation in smectite and illite formation (Siyuan and Stucki 1994; Stucki 1997). This Fe reduction is partially reversed in the dry periods but increases in every complete cycle, and the process is efficient (Siyuan and Stucki 1994; Stucki 1997). The reason why reduction is never completely reversed is probably related to water inaccessibility to collapsed, K-exchanged layers. Norrish and Pickering (1983) observed that authigenic illites from Australian soils have an average higher Fe content than illites derived from mica alteration. This difference may be an indication that only smectite with intermediate to high Fe content can be transformed into illite in soil conditions and, hence, only authigenic illites with such Fe content are found in soils. It is expected that the extent of illitization will be proportional to the Fe content in smectite. This is what we observe in our samples. Although there are no chemical analyses available of the I-S phase of samples –80 and +44, the relative Fe content in the specimens can be obtained from the positions of some of the XRD peaks in the powder patterns. We measured such positions for the 060; 020,110; and 200, $\bar{1}31$ peaks, which correlated well and indicated an increasing **b** parameter in the sequence +80, +940, –1200, +120 < –80 < +44. The correlation between the 060

and 200, $\bar{1}31$ peak positions is shown in Figure 10 (top). The **b** parameter (proportional to *d*[060]) increases with both total Fe content and the Fe^{2+}/Fe^{3+} ratio, due to the larger radius of Fe^{2+}. The sequence of the **b** parameter increase is in agreement with the overall illite contents in the samples, as shown also in Figure 10 (middle). Finally, the Fe^{2+} content is also well correlated with illite content (Fig. 10, bottom). The fact that sample +80 has ~8% too few illite layers from the trend indicated by the other samples may be due to a significant smaller illite layer proportion in the original, detrital I-S. The similarity between the middle and bottom plots in Figure 10 indicates that sample –80 should appear in the shaded area (bottom plot), strengthening the correlation between Fe^{2+} and illite layers contents.

These results show a general positive correlation between illite and Fe content. However, our modeling of oriented mount XRD patterns requires the most illitic phase in each sample to have a lower Fe content than the less illitic components, except for +44 (Table 1). These two facts are not incompatible because Fe depletion may happen in each phase only at the end of illitization, as a result of a lattice stabilization process of illite layers that is much slower than smectite illitization. However, further and direct evidence of such Fe depletion is needed.

The proposed mechanism explains why the intermediate products are so heterogeneous, with I-S of many different compositions in each sample (Figs. 3 and 4, Table 1). The development of layer charge will depend on the layer charge of the original smectite layers and their Fe content, which are known to be heterogeneous. Because atom mobility is minimal or null, the heterogeneity will be maintained along the transformation. This mechanism also explains that only *R*0 interstratification develops (at least up to 85% illite in I-S) because the low atom mobility does not allow the development of the more stable *R*1 interstratification. Layer collapse and illite formation is only dependent on Fe abundance and initial layer charge, and both these variables have random values across smectite layers.

Our samples have remarkable similarities with those described by Deconinck et al. (1988). The environments of deposition are similar; both have intermediate Fe contents and random layer stacking ($1M_d$ polytype). Their I-S specimens have 90% or more illite and it is impossible to differentiate between *R*0 and *R*>0 order, although those authors indicated that there could be some admixture of illite and an I-S phase. If the latter is true, their I-S would also show a heterogeneous composition. Certainly, their DTA curves reveal a large dehydration reaction at ~100 °C that suggests the presence of a significant number of smectite layers because illite retains very little hydration (adsorbed) water. The main dehydroxylation event in the I-S of Deconinck et al. (1988) occurs at ~500 °C, as in our samples. In our study, I-S presents several dehydroxylation events from 500 to 700 °C (Fig. 8), which is an indication of heterogeneity in the composition of the octahedral sheets. Aluminum-rich, cis-vacant I-S dehydroxylates at 600–650 °C, whereas the trans-vacant counterpart does at 500–550°C (Drits et al 1995; Cuadros and Altaner 1998a). As Fe content increases, however, dehydroxylation of cis-vacant layers occurs at lower temperature (Heller-Kalai and Rozenson 1980; Muller et al. 2000). Probably, our multiple dehydroxylation events are due to variable Fe content in the cis-vacant I-S layers.

Wider implications and relevance

Previous evidence (Watts 1980; Singer and Stoffers 1980; Robinson and Wright 1987; Deconinck et al. 1988; Gilg et al. 2003) and the present work indicate that smectite can be transformed into I-S and illite at surface temperature by wetting and drying cycles. We believe that we have demonstrated that the driving force in this process is Fe reduction. In the environment where our samples were transformed, Fe reduction must have been produced by bacteria that would be active during the waterlogged periods and inactive during periods when the soil was dry. This has implications for palaeoclimatology and stratigraphy and relevance to soil science.

Since the illitization occurs during periods of high seasonality, it can be used as an indication of seasonal palaeoclimate. Huggett et al. (2001) used the relationship between seasonality and astronomical cycles to tune high illitic clay values to eccentricity maxima, and hypothesized that conspicuous groups of high illitic clay peaks correspond with long eccentricity (400 Ka) maxima. The distribution of illite-rich pedogenic or lacustrine clay can therefore be used to better constrain the relative dating of non-marine sediment. The illite-derived maxima can be anchored to the global chronostratigraphical scale using magnetostratigraphy.

Potassium (and NH_4) fixation by smectite in soils subjected to wetting and drying has implications for soil fertility. It is known that soils can become enriched in illite through K and NH_4 fixation when subjected to fluctuating redox conditions caused by wetting and drying (Stucki 1997; Velde 2003). Our and their data suggest that this process is driven by Fe-reduction. Although this has not been recorded for the soils investigated by Velde (2003), he suggested that organic matter, the most widely available reducing agent in soils, is critical to clay transformation reactions in this environment.

The ability of microorganisms to reduce structural Fe in clays has become recognized as an important mechanism for the oxidation of pollutants in soils. Ernstsen et al. (1998) suggest that Fe reduction on weathered, oxidized clay minerals may be a renewable source of reduction capacity in imperfectly drained soils. Both our results and those of Ernstsen et al. suggest that the significance of such processes will depend upon the abundance of detrital Fe-rich smectite.

Acknowledgments

We thank S. Fiore for providing the TG analyses. We are also grateful to A. Meunier and M. Jaboyedoff for their careful review of the manuscript and insightful comments.

References cited

Armenteros, I., Daley, B., and Garcia, E. (1997) Lacustrine and palustrine facies in the Bembridge Limestone (late Eocene, Hampshire Basin) of the Isle of Wight, southern England. Palaeogeography, Palaeoclimatology, Palaeoecology, 128, 111–132.

Cuadros, J. (2002) Structural insights from the study of Cs-exchanged smectites submitted to wetting-and-drying cycles. Clay Minerals, 37, 473–486.

Cuadros, J. and Altaner, S.P. (1998a) Compositional and structural features of the octahedral sheet in mixed-layer illite/smectite from bentonites. European Journal of Mineralogy, 10, 111–124.

——— (1998b) Characterization of mixed-layer illite-smectite from bentonites using microscopic, chemical, and X-ray methods: Constraints on the smectite-to-illite transformation mechanism. American Mineralogist, 83, 762–774.

Daley, B. (1999) Palaeogene sections on the Isle of Wight. A revision of their description and significance in the light of research undertaken over recent decades. Tertiary Research, 19, 1–69.

Deconinck, J.F., Strasser, A., and Debrabant, P. (1988) Formation of illitic minerals at surface temperatures in Purbeckian sediments (lower Berriasian, Swiss and French Jura). Clay Minerals, 23, 91–103.

Drits, V.A., Besson, G., and Muller, F. (1995) An improved model for structural transformations of heat-treated aluminous dioctahedral 2:1 layer silicates. Clays and Clay Minerals, 43, 718–731.

Drits, V., Salyn, A., and Šucha, V. (1996) Structural transformations of interstratified illite-smectites from Dolná Ves hydrothermal deposits: dynamics and mechanisms. Clays and Clay Minerals, 44, 181–190.

Eberl, D., Środoń, J., and Northrop, R. (1986) Potassium fixation in smectite by wetting and drying. In J.A. Davis and K.F. Hayes, Eds., ACS Symposium Series 323, p. 296–326. American Chemical Society, Washington, D.C.

Ernstsen, V., Gates, W.P., and Stucki, J.W. (1998) Microbial reduction of structural iron in clays - A renewable source of reduction capacity. Journal of Environmental Quality, 27, 761–766.

Fitzpatrick, E.A. (1980) Soils, their formation, classification and distribution, 345 p. Longman, London.

Gabis, V. (1963) Etudes minéralogique et géochemique de la série sédimentaire Oligocene du Velay. Bulletin de liaison de la Société Française de Minéralogie et de Cristallographie, 84, 315–354.

Gale, A.S., Jeffery, P.A., Huggett, J.M., and Connolly, P. (1999) Eocene inversion history of the Sandown Pericline, Isle of Wight, southern England. Journal of the Geological Society London, 156, 327–339.

Gilg, H., Weber, B., Kasbohm, J., and Frei, R. (2003) Isotope geochemistry and origin of illite-smectite and kaolinite from the Seilitz and Kermmlitz kaolin deposits, Saxony, Germany. Clay Minerals, 38, 95–112.

Gilkes, R.J. (1968) Clay mineral provinces in the Tertiary sediments of the Hampshire Basin. Clay Minerals, 7, 351–361.

Hay, R.L., Guldman, S.G., Mathews, J.C., Lander, R.H., Duffin, M.E., and Kyser, T.K. (1991) Clay mineral diagenesis in core KM-3 of Searles Lake, California. Clays and Clay Minerals, 39, 84–96.

Heller-Kallai, L. and Rozenson, I. (1980) Dehydroxylation of dioctahedral phyllosilicates. Clays and Clay Minerals, 28, 355–368.

Huggett, J.M., Gale, A.S., and Clauer, N. (2001) Nature and origin of non-marine 10 Å clay from the Late Eocene and Early Oligocene of the Isle of Wight (Hampshire Basin), U.K. Clay Minerals, 36, 447–464.

Inoue, A. and Utada, M. (1983) Further investigations of a conversion series of dioctahedral mica/smectites in the Shinzan hydrothermal alteration area, northeast Japan. Clays and Clay Minerals, 31, 401–412.

Mackenzie, R.C. (1957) The Differential Thermal Investigation of Clays, 456 p. Mineralogical Society, London.

Mamy, J. and Gaultier, J.P. (1975) Etude de l'evolution de l'ordre cristallin dans la montmorillonite en relation avec la diminution d'echangeabilite du potassium. Proceedings of the International Clay Conference, 149–155.

Moore, D.M. and Reynolds, R.C. (1997) X-ray Diffraction and the Identification and Analysis of Clay Minerals, 378 p. Oxford University Press, Oxford.

Muller, F., Drits, V., Plançon, A., and Robert, J.-L. (2000) Structural transformation of 2:1 dioctahedral layer silicates during dehydroxylation-rehydroxylation reactions. Clays and Clay Minerals, 48, 572–585.

Norrish, K. and Pickering, J. (1983) Clay Minerals. In Soils, an Australian viewpoint, p. 281–308. CSIRO/Academic Press, Melbourne, Australia.

Ollier, C. and Pain, C. (1996) Soils and Landforms, 316 p. Wiley, Chichester.

Paul, C.R.C. (1989) The molluscan faunal succession in the Hatherwood Limestone Member (Upper Eocene), Isle of Wight. Tertiary Research, 10, 147–162.

Reynolds, R.C., Jr. (1993) Three-dimensional X-ray powder diffraction from disordered illite: simulation and interpretation of the diffraction patterns. In R.C. Reynolds and J.R. Walker, Eds., Computer Applications to X-ray Powder Diffraction Analysis of Clay Minerals, p. 44–78. CMS Workshop Lectures, vol. 5. Clay Minerals Society, Boulder, Colorado.

Reynolds, R.C., Jr. and Reynolds, R.C., III (1996) NEWMOD: The Calculation of One-Dimensional X-ray Diffraction Patterns of Mixed-Layered Clay Minerals. Computer Program. 8 Brook Road, Hanover, New Hampshire.

Robinson, D. and Wright, V.P. (1987) Ordered illite-smectite and kaolinite-smectite: pedogenic minerals in a lower Carboniferous paleosol sequence, South Wales? Clay Minerals, 22, 109–118.

Sakharov, B.A., Lindgreen, H., Salyn, A., and Drits, V.A. (1999) Determination of illite-smectite structures using multispecimen X-ray diffraction profile fitting. Clays and Clay Minerals, 47, 555–566.

Singer, A. (1984) The Paleoclimatic Interpretation of Clay Minerals in Sediments—a Review. Earth-Science Reviews, 21, 251–293.

Singer, A. and Stoffers, P. (1980) Clay Mineral diagenesis in two East African lake sediments. Clay Minerals, 15, 291–307.

Siyuan, S. and Stucki, J. (1994) Effects of iron oxidation state on the fate and behaviour of potassium in soils. In: Soil Testing: Prospects for Improving Nutrient Recommendations, p. 173–185. Soil Science Society of America Special Publication 40.

Stucki, J. (1997) Redox processes in smectites: Soil environmental significance. Advances in GeoEcology, 30, 395–406.

Šucha, V. and Širáňová, V. (1991) Ammonium and potassium fixation in smectite by wetting and drying. Clays and Clay Minerals, 39, 556–559.

Velde, B. (2003) Fast action in soils: Kinetics of clay mineral change under conditions of agriculture and the role of organic matter, p. 278. Euroclay 2003 Abstracts, 10th Conference of the European Clay Groups Association, Modena, Italy.

Watts, N.L. (1980) Quaternary pedogenic calcretes from the Kalahari (southern Africa): mineralogy, genesis and diagenesis. Sedimentology, 27, 661–686.

Manuscript received April 19, 2004
Manuscript accepted January 18, 2005
Manuscript handled by Michael Fechtelkord